FULL PAPER

BN–Graphene Composites Generated by Covalent Cross-Linking with Organic Linkers

*Ram Kumar, K. Gopalakrishnan, Irshad Ahmad, and C. N. R. Rao**

Composites of boron nitride (BN) and carboxylated graphene are prepared for the first time using covalent cross-linking employing the carbodiimide reaction. The $BN_{1-x}G_x$ ($x \approx 0.25$, 0.5, and 0.75) obtained are characterized using a variety of spectroscopic techniques and thermogravimetric analysis. The composites show composition-dependent electrical resistivity, the resistivity decreasing with increase in graphene content. The composites exhibit microporosity and the $x \approx 0.75$ composite especially exhibits satisfactory performance with high stability as an electrode in supercapacitors. The $x \approx 0.75$ composite is also found to be a good electrocatalyst for the oxygen reduction reaction in fuel cells.

1. Introduction

Hexagonal boron nitride (*h*-BN) is a layered insulator while graphene is a layered conductor. Although *h*-BN nanosheets and graphene are isoelectronic with the same layered structure, there are essential differences in the chemistry and properties of BN nanosheets. Numerous potential applications of these two nanomaterials have been reported in the recent literature.[1] Composites of BN and graphene are expected to be materials of great interest and there have been efforts to study ternary borocarbonitrides, $B_xC_yN_z$ with varying carbon content.[2] Synthesis of few-layer BCN has been achieved by solid state chemistry route and chemical vapor deposition (CVD) techniques.[2b,3] These systems consist of hybridized, randomly distributed domains of BN, and graphene phases with variable composition. By varying the carbon content optical, electrical and other functional properties of the borocarbonitrides can be tuned.[2a,3b,4] There has also been effort to deposit BN sheets over graphene and vice versa.[2a,5] Two different approaches have been employed to prepare such hybrid heterostructures of BN and graphene. Graphene and BN nanosheets were prepared by exfoliation of graphite powder and bulk *h*-BN. Subsequently graphene and BN were mixed and self-assembled using van der Waals interaction.[6] The second approach involves sequential CVD growth of BN and graphene on a substrate.[5] We have been interested in preparing hybrid composites of BN and graphene with different compositions by covalent cross-linking using organic linkers. We have recently used covalent cross-linking to prepare assemblies of single-walled carbon nanotubes as well as graphene.[7] Graphene-BN composites prepared by covalent cross-linking would be expected to possess properties different from those obtained by depositing BN and graphene sheets on each other. We have prepared $BN_{1-x}G_x$ composites with varying graphene content (x = 0–1) and studied their electrical properties. Since heavily nitrogenated graphene as well as borocarbonitrides are reported to show good characteristics as electrodes in supercapacitors as well as in the oxygen reduction reaction (ORR),[8] we have investigated the use of the $BN_{1-x}G_x$ composites in supercapacitors and as catalysts in the ORR in fuel cells.

R. Kumar, K. Gopalakrishnan, Dr. I. Ahmad, Prof. C. N. R. Rao
Chemistry and Physics of Materials Unit
New Chemistry Unit
Sheikh Saqr Laboratory, International Centre for Materials Science (ICMS) and CSIR Centre of Excellence in Chemistry
Jawaharlal Nehru Centre for Advanced Scientific Research
Jakkur P.O., Bangalore 560064, India
E-mail: cnrrao@jncasr.ac.in

DOI: 10.1002/adfm.201502166

2. Results and Discussion

Scheme 1 shows the steps involved in the synthesis of the amide bond cross-linked assemblies of BN and graphene ($BN_{1-x}G_x$, $x \approx 0.25$, 0.5, 0.75). Carboxylate functionalized graphene (G), obtained by microwave irradiation of graphene in a HNO_3/H_2SO_4 mixture,[9] was reacted with amine-functionalized few-layer BN (≈1–4 layers) prepared by heating boric acid and urea in 1:48 molar ratio in an ammonia atmosphere.[10] We have employed the carbodiimide method to link BN and G with amide bond, by using EDC {1-ethyl-3-(3-dimethylaminopropyl) carbodiimide)} as the reagent (see the Experimental Section for details).[11] The advantage of EDC coupling over $SOCl_2$-based activation is that no HCl is liberated and urea obtained as a by-product is water-soluble. Three different compositions of the $BN_{1-x}G_x$ composites ($x \approx 0.25$, 0.5, 0.75) were obtained by varying the ratio of BN with respect to graphene.

We have examined the $BN_{1-x}G_x$ composites using electron microscopy. **Figure 1** shows typical electron microscope images of few-layer BN, carboxylated graphene, and $BN_{0.5}G_{0.5}$. Transmission electron microscopy (TEM) images of few-layer BN and carboxylated graphene show wrinkled transparent sheets. TEM and scanning electron microscopy (SEM) images of the $BN_{1-x}G_x$ composites show layer-by-layer self-assembly of the component sheet structures. (Figure 1 and Figure S2, Supporting Information). The layer-by-layer self-assembly

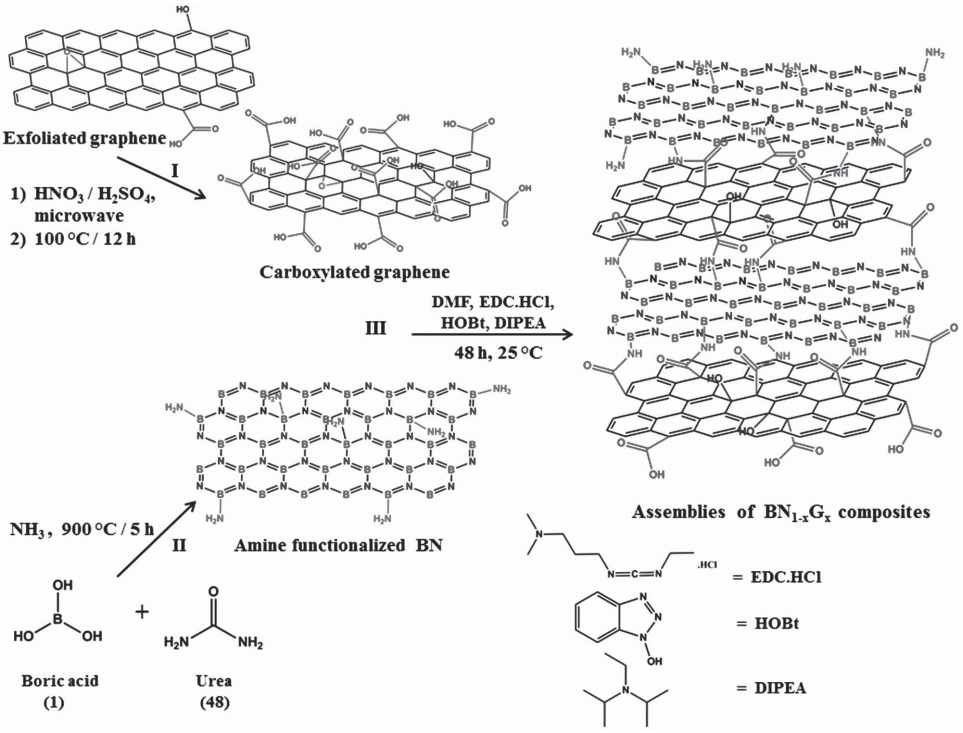

Scheme 1. Schematic representation of the synthesis of covalently cross-linked assemblies of BN and graphene using EDC coupling. I) Synthesis of carboxylated graphene; II) synthesis of amine functionalized few-layer BN; III) Synthesis of assemblies of $BN_{1-x}G_x$ composites by amide bond cross-linking using EDC coupling.

of graphene and BN is facilitated by amide bond formation between the amine group on the BN sheets and the carboxylate groups on the graphene sheets. Elemental mapping of the $BN_{1-x}G_x$ using energy-dispersive X-ray spectroscopy (EDAX) shows uniform distribution of B, N, and C confirming homogeneous nature of the composite (**Figure 2** and Figure S3, Supporting Information).

The electron energy loss spectrum (EELS) of $BN_{0.5}G_{0.5}$ displayed in Figure S4 (Supporting Information) shows the K shell ionization edges of B, N, C, and O respectively. The K-shell ionization edge at 192.6 eV is due to the transition of B 1s electron to the π^* antibonding orbitals, associated with planar bonding and sp^2 hybridization of boron. The signals in the 200–216 eV range are due to the 1s → σ^* transition of boron. The N EEL

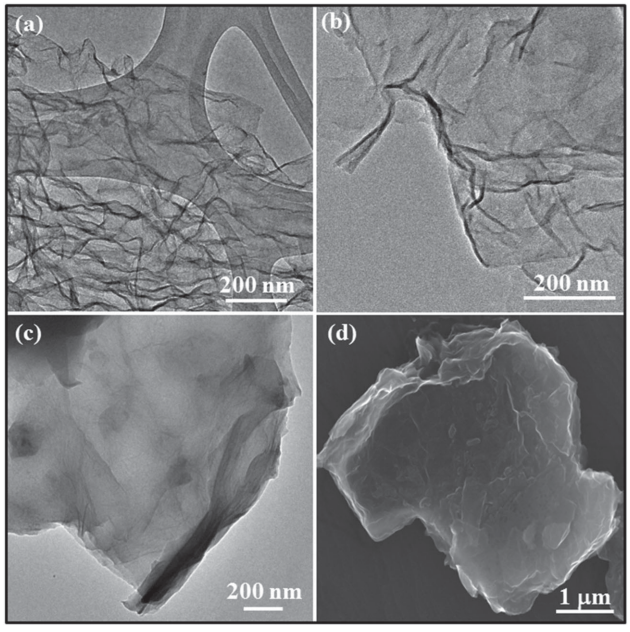

Figure 1. TEM images of: a) few-layer BN, b) carboxylated graphene, c) and d) TEM and SEM images of $BN_{0.5}G_{0.5}$.

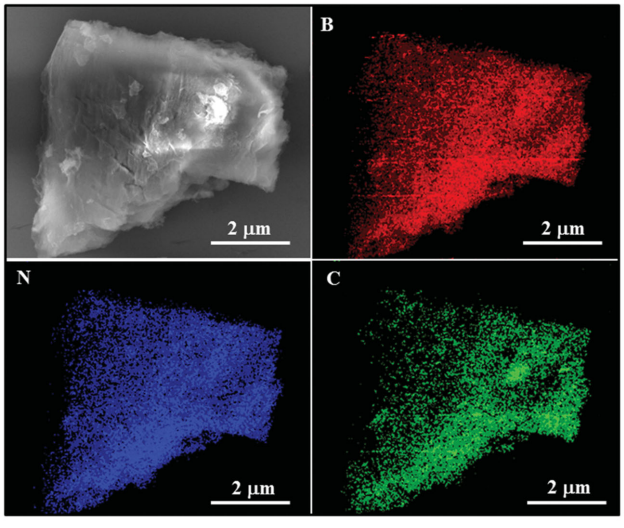

Figure 2. Elemental mapping of $BN_{0.5}G_{0.5}$. B (red), N (blue), and C (green).

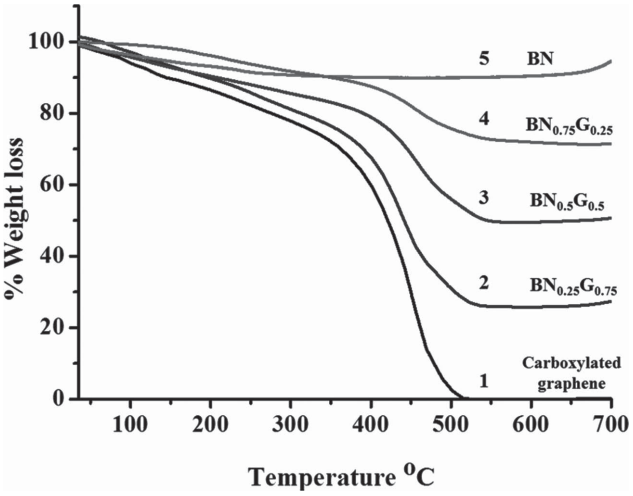

Figure 3. Thermogravimetric analysis of carboxylated graphene (1), $BN_{0.25}G_{0.75}$ (2), $BN_{0.5}G_{0.5}$ (3), $BN_{0.75}G_{0.25}$ (4), and BN (5) in an oxygen atmosphere.

spectrum has peaks at 402.5 eV assigned to 1s → π^* transition, whereas peaks at 409 and 416 eV are due to 1s → σ^* transition of BN.[12] The C K shell ionization edge has bands at 286 and 296 eV corresponding to 1s → π^* and 1s → σ^* transitions of graphene.[12a,13] The O K shell ionization is also observed at 541 eV due to oxygen containing functional groups in the composite.[14] Core level X-ray photoelectron spectra (XPS) of $BN_{0.5}G_{0.5}$ are shown in Figure S5 (Supporting Information). The B 1s core level has main peak at 190.7 eV corresponding to B–N bonding along with two minor contributions at 188.8 eV and 192.7 eV due to interaction of B with C and O of graphene basal plane.[15] The N 1s core level has signal at 398 eV due to bonding with B. The peak at 400.5 eV is due to N of amide groups on the BN basal plane.[10c,15a] The C 1*s* core level spectrum shows signals at 284.6 and 288 eV due to graphene (sp^2) and amide carbons.[16] The carboxylate functionalization of graphene involves HNO_3/H_2SO_4 treatment, which introduces minor density of epoxide and hydroxyl groups. This is reflected as additional broadness of the C 1s spectrum. The Peak at 286.4 eV has contributions from sp^3 C along with a minor concentration of epoxide and hydroxyl groups. The presence of unreacted carboxylate is reflected as minor contribution at 289 eV.[16a] ^{13}C and ^{11}B solid state nuclear magnetic resonance spectra (NMR) of $BN_{0.5}G_{0.5}$ collected at 20 and 14 kHz magic angle spinning (MAS) respectively show characteristics of aromatic sp^2 carbon, *h*-BN, and other features expected of the composite (Figure S6, Supporting Information).[17] Further separation of few-layers and homogeneous mixing of BN and graphene is expected in *N,N*-dimethylformamide (DMF) due to sonication.[6,18] The EDC coupling reagents activate the carboxylate groups on the graphene basal plane and the activated carboxylate groups direct the assembly by allowing amide bond formation with BN. We believe that such covalent cross-linking results in greater homogeneity and better control of the structure of composite. It is possible that two or three layers of graphene are sandwiched between BN sheets or vice versa. Powder X-ray diffraction patterns (PXRD) of the $BN_{1-x}G_x$ composites show reflections due to the (002) planes suggesting the turbostatic ordering of BN and graphene.

Thermogravimetric analysis was carried out in an oxygen atmosphere to determine the compositions of the composites (**Figure 3**). Few-layer BN has high thermal stability with no weight loss in the 500–700 °C range. The thermogravimetric analysis (TGA) profile of carboxylated graphene shows complete combustion in the 400–500 °C temperature range. The BN content in the composites can be determined from the residual weight in this temperature range. The residual weight for $BN_{0.25}G_{0.75}$, $BN_{0.5}G_{0.5}$, and $BN_{0.75}G_{0.25}$ are 24%, 49.5%, and 72% respectively, which match with the stated compositions.

The infrared spectrum of few-layer BN shows two strong and broad bands at 800 and 1367 cm^{-1} corresponding to the out-of-plane B—N—B bending mode (A_{2u}) and the in-plane B—N transverse optical mode (E_{1u}), respectively (**Figure 4**a).[19] Carboxylated

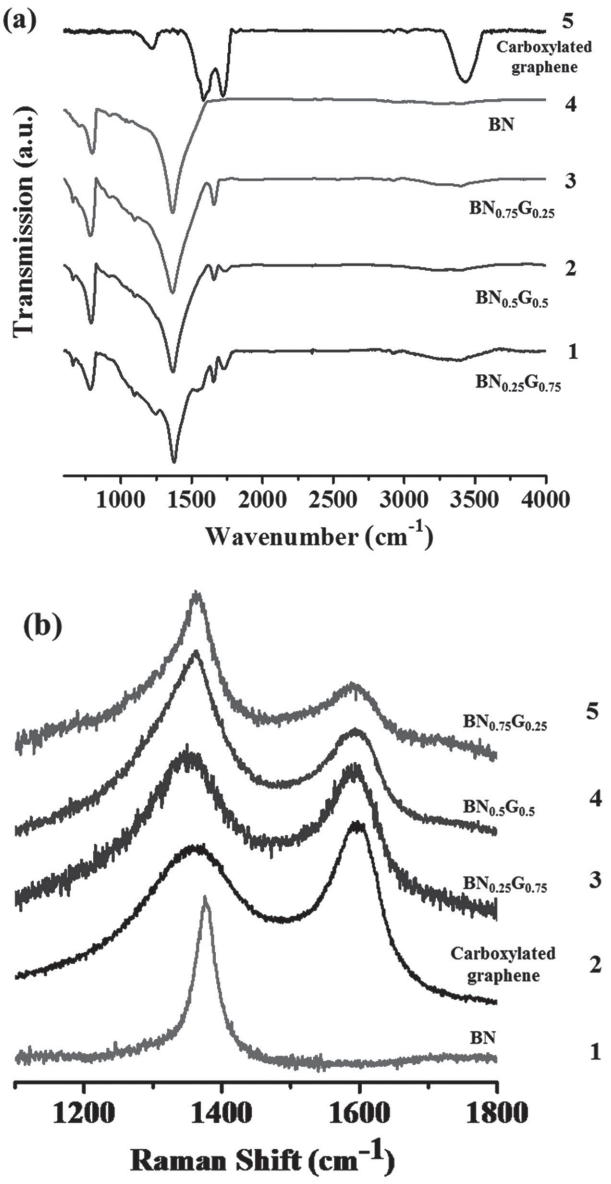

Figure 4. a) Infrared spectra of $BN_{0.25}G_{0.75}$ (1), $BN_{0.5}G_{0.5}$ (2), $BN_{0.75}G_{0.25}$ (3), BN (4), and carboxylated graphene (5). b) Raman Spectra of BN (1), carboxylated graphene (2), $BN_{0.25}G_{0.75}$ (3), $BN_{0.5}G_{0.5}$ (4), and $BN_{0.75}G_{0.25}$ (5).

graphene has IR bands at 1576, 1723, and 3450 cm^{-1} assigned to aromatic C=C, C=O, and O—H stretching of carboxylate groups. The weak band around 1250 cm^{-1} is attributed to the C—O stretching of epoxide and hydroxyl groups on graphene. [20] IR spectra of $BN_{1-x}G_x$ composites have bands at 1653 and 1724 cm^{-1} due to the amide bond between graphene and BN nanosheets and remaining carboxylate group on the graphene basal plane (Figure 4a).[20] As the amount of BN in the composites increases the relative intensity of the 1653 cm^{-1} amide band increases, $BN_{0.75}G_{0.25}$ showing an almost negligible intensity of the 1724 cm^{-1} band. The band around 1250 cm^{-1} of the composites disappears on heating at 300 °C. The Raman spectrum of few-layer BN has a relatively narrow (≈35 cm^{-1}) band at 1375 cm^{-1} corresponding to the E_{2g} mode of BN (Figure 4b and Figure S7, Supporting Information).[21] Carboxylated graphene shows the characteristic D and G bands at 1359 and 1593 cm^{-1} with line widths of 165 and 75 cm^{-1}, respectively.[22] Raman spectra of composites have features of both BN as well as graphene (Figure 4b and Figure S7, Supporting Information). As the BN content increases in the $BN_{1-x}G_x$ composites, the spectrum shows dominating BN feature and decrease in G-band intensity.

Surface area and porosity of the $BN_{1-x}G_x$ composites were obtained by N_2 adsorption at 77 K (**Figure 5**). The Brunauer–Emmet–Teller (BET) surface areas of $BN_{0.25}G_{0.75}$, $BN_{0.5}G_{0.5}$, and $BN_{0.75}G_{0.25}$ are 183, 171, and 197 $m^2\ g^{-1}$, respectively. The sorption profiles show type H4 hysteresis loop associated with narrow slit-like pores, with type-I isotherm character in the low pressure region indicative of microporosity according to the International Union of Pure and Applied Chemistry (IUPAC) classification.[23] Slit-like micropores are created due to cross-linking and stacking of BN and graphene sheets. Carboxylated graphene has a BET surface area of 38 $m^2\ g^{-1}$ with type-IV mesoporous sorption profile due to agglomeration of graphene sheets (Figure S8a, Supporting Information). Few-layer BN has type-II sorption profile with BET surface area of 452 $m^2\ g^{-1}$ (Figure S8b, Supporting Information).

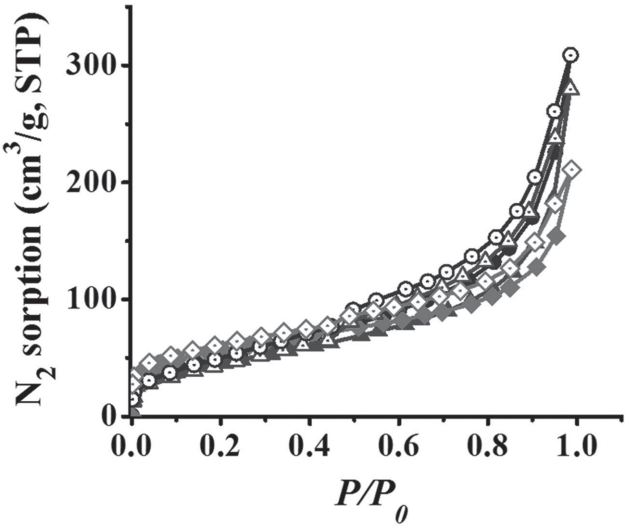

Figure 5. Nitrogen sorption profile of $BN_{0.25}G_{0.75}$ (circles), $BN_{0.5}G_{0.5}$ (triangles), and $BN_{0.75}G_{0.25}$ (diamonds) at 77 K.

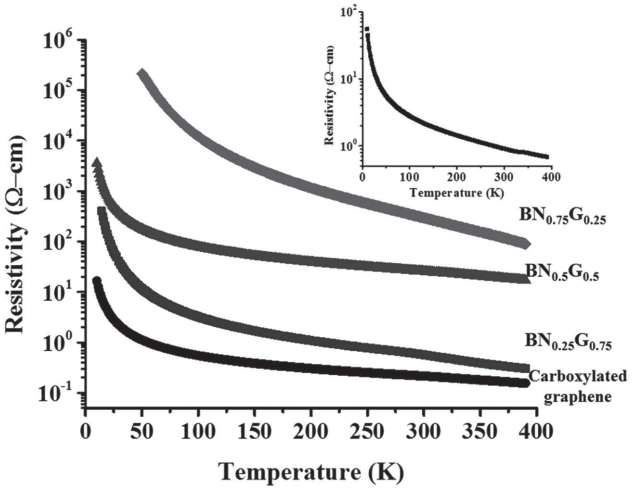

Figure 6. Temperature dependence of resistivity in $BN_{1-x}G_x$ composites (measured using four-probe method). Inset: Temperature-dependent resistivity of $BN_{0.5}G_{0.5}$ on annealing at 300 °C in a nitrogen atmosphere.

Electrical resistivity data of the $BN_{1-x}G_x$ composites are shown in **Figure 6**. The $BN_{1-x}G_x$ composites show typical semiconducting behavior with the resistance decreasing on increasing the temperature. The resistivity of the composites is least in the case of $BN_{0.25}G_{0.75}$ and increases on increasing the BN content. This is expected since BN is a known large band gap insulator. This interesting variable resistivity suggests the possible use of different $BN_{1-x}G_x$ composites for various potential applications. The resistivity of $BN_{0.5}G_{0.5}$ decreases significantly on annealing at 300 °C (see inset of Figure 6) due to the loss of the amide linkers (Figure S9, Supporting Information).

Presence of a slit-like microporous network in the $BN_{1-x}G_x$ composites prompted us to investigate the performance of $BN_{1-x}G_x$ as supercapacitor electrode material. Electrochemical performance of the $BN_{1-x}G_x$ composites was investigated by means of cyclic voltammetry (CV), galvanostatic charge–discharge (GCD) curves, and electrochemical impedance spectroscopy (EIS) in 2 M H_2SO_4 electrolyte. Cyclic voltammograms of carboxylated graphene, $BN_{0.25}G_{0.75}$, $BN_{0.5}G_{0.5}$, and $BN_{0.75}G_{0.25}$ are measured at different scan rates (2–100 mV s^{-1}) at a voltage window of –0.2–0.6 V. The CV curves measured at 40 mV s^{-1} are shown in **Figure 7**a. The CV curves show a rectangular feature even at higher scan rates which indicates that these materials are good charge storage supercapacitor electrodes. We have found a maximum capacitance of 217 F g^{-1} at a scan rate of 2 mV s^{-1} in the case of $BN_{0.25}G_{0.75}$. The specific capacitance values of carboxylated graphene, $BN_{0.5}G_{0.5}$, and $BN_{0.75}G_{0.25}$ are 89, 180, 92 F g^{-1}, respectively, at 2 mV s^{-1}. The galvanostatic charge–discharge curves of the BNG samples were measured in a voltage window from –0.2 to 0.6 V at different current densities. Figure 7b shows the charge–discharge curves of carboxylated graphene and $BN_{1-x}G_x$ composites measured at 1 A g^{-1}. The discharge time of $BN_{0.25}G_{0.75}$ was longer when compared to carboxylated graphene and other two composites. The charge–discharge curves look symmetric for the $BN_{1-x}G_x$ composites resembling those of ideal capacitors. The specific capacitance values decrease with increase in the current density as shown in Figure 7c. The specific capacitance of $BN_{0.25}G_{0.75}$,

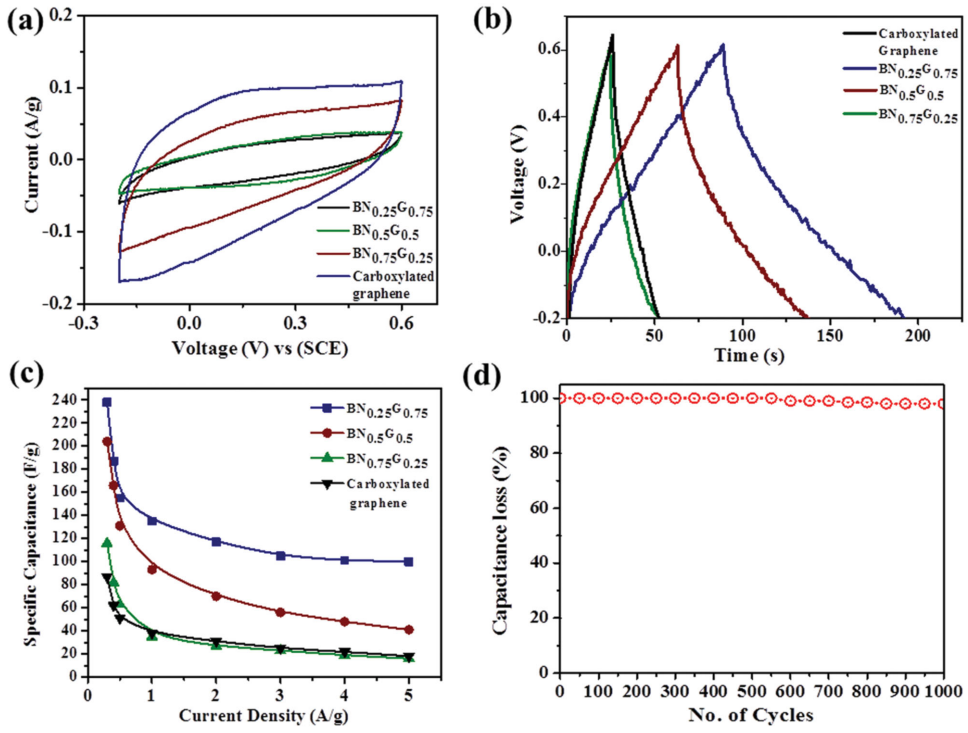

Figure 7. a) Cyclic voltammograms of carboxylated graphene and $BN_{1-x}G_x$ electrodes at a scan rate of 40 mV s^{-1}. b) Galvanostatic charge–discharge curves for carboxylated graphene and $BN_{1-x}G_x$ electrodes (at 1 A g^{-1}); c) Specific capacitance as a function of discharge current, and d) % capacitance loss versus the cycle number of $BN_{0.25}G_{0.75}$ measured at a current density of 1 A g^{-1} within an operational window from –0.2 to 0.6 V. Aqueous 2 M H_2SO_4 solution used as electrolyte.

$BN_{0.5}G_{0.5}$, and $BN_{0.75}G_{0.25}$ is 238, 204, and 116 F g^{-1}, respectively, at 0.3 A g^{-1}, while carboxylated graphene alone exhibits a value of 87 F g^{-1}. The high specific capacitance of $BN_{1-x}G_x$ is attributed to the enhanced surface area along with the presence of slit-like microporous channels created in the composite due to covalent cross-linking.

We have studied the cycling stability for $BN_{0.25}G_{0.75}$ by charge–discharge experiments between –0.2 and 0.6 V at a current density of 1 A g^{-1} for 1000 cycles. $BN_{0.25}G_{0.75}$ showed a loss of only ≈2% from the initial specific capacitance with excellent stability and capacitance retention (Figure 7d). BN has exceptionally high chemical and thermal stability; its presence in the conductive graphene matrix provides synergistic interactions with high electrochemical stability. We show the Nyquist plots in the frequency range 100 kHz–0.01 Hz in **Figure 8**. These plots show excellent capacitive behavior of the $BN_{1-x}G_x$ composites as indicated by the near vertical line over the lower frequency range. The charge transfer resistance (C_t) in $BN_{0.25}G_{0.75}$, $BN_{0.5}G_{0.5}$, and $BN_{0.75}G_{0.25}$ is small and the equivalent series resistances (ESRs) are 26.7, 29.0, and 45.3 Ω, respectively. The specific capacitance increases with increasing graphene content going up to ≈200 F g^{-1} for $BN_{0.25}G_{0.75}$ and $BN_{0.5}G_{0.5}$. It is noteworthy that the resistivity decreases in the same order although the surface area remains nearly constant.

We have investigated the electrocatalytic activity of carboxylated graphene and $BN_{1-x}G_x$ composites in the ORR by CV at a slow scan rate of 5 mV s^{-1} in O_2-saturated and N_2-saturated

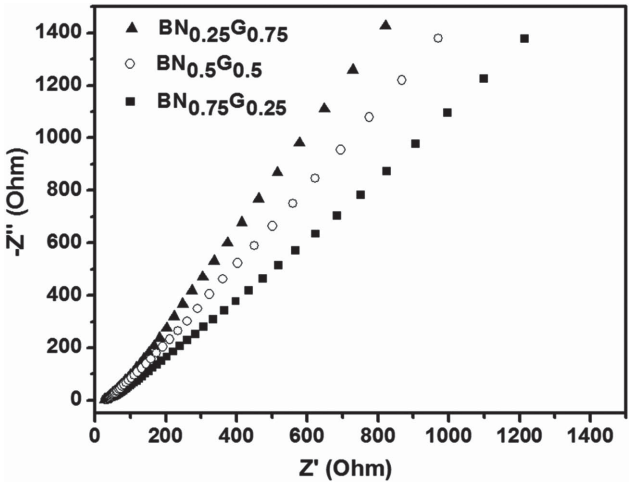

Figure 8. Nyquist plot for $BN_{1-x}G_x$ electrodes.

0.1 M KOH electrolytes, using a conventional three-electrode system (**Figure 9**a). The $BN_{1-x}G_x$ composites show cathodic peaks ranging from –0.25 to –0.35 V versus standard calomel electrode (SCE) in an O_2-saturated electrolyte, indicating a good O_2 reduction property whereas carboxylated graphene does not show a prominent reduction peak. This shows that addition of BN to graphene assists the reduction of oxygen. Linear-sweep voltammetry (LSV) of carboxylated graphene and $BN_{1-x}G_x$ composites at a rotation speed of 1600 rpm is

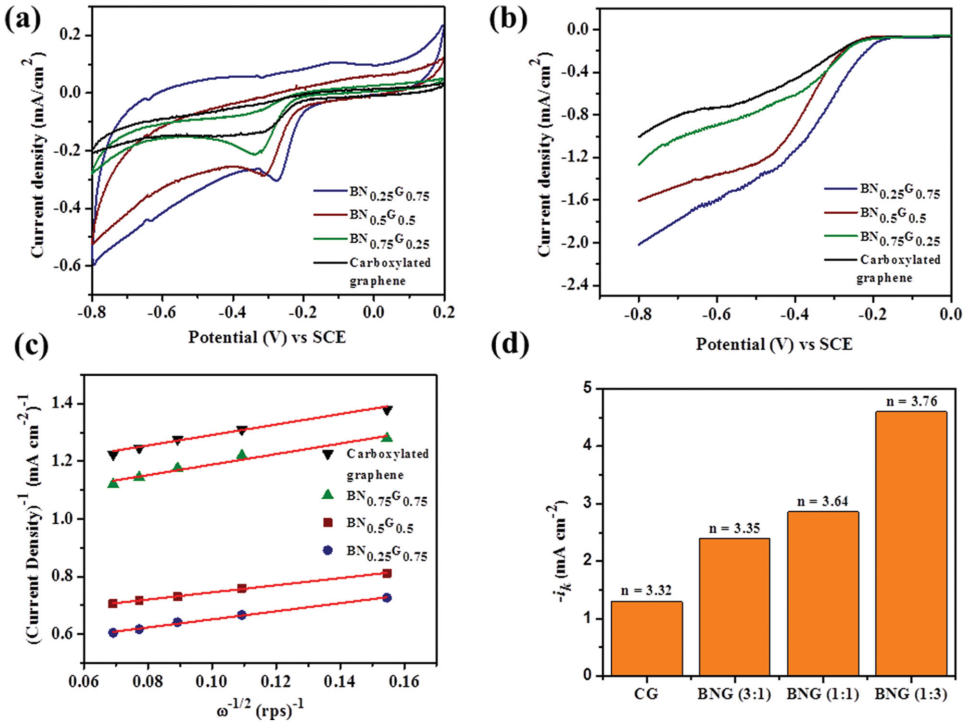

Figure 9. a) Cyclic voltammetry curves of carboxylated graphene and $BN_{1-x}G_x$ composites in oxygen saturated 0.1 M KOH with a scan rate of 5 mV s^{-1}. b) LSV curves of EG and $BN_{1-x}G_x$ composites in oxygen saturated 0.1 M KOH with a scan rate of 5 mV s^{-1} and a rotation rate of 1600 rpm. c) Koutecky–Levich plots obtained at –0.6 V versus SCE, and d) variation of kinetic current density (i_k) at –0.4 V versus SCE for EG and $BN_{1-x}G_x$ composites. Aqueous 0.1 M KOH solution used as electrolyte.

displayed in Figure 9b. The $BN_{1-x}G_x$ composites exhibit higher current density on addition of graphene to BN representing an enhanced activity for ORR. $BN_{0.25}G_{0.75}$ shows a more positive onset potential than $BN_{0.5}G_{0.5}$, $BN_{0.75}G_{0.25}$, and carboxylated graphene. The Koutecky–Levich plots (i^{-1} vs $\omega^{-1/2}$) were obtained from the polarization curves at a potential of –0.6 V versus SCE for all the catalysts as shown in Figure 9c. The transferred electron number (n) per O_2 calculated from the slopes of Koutecky–Levich plots ranges from 3.3 to 3.8. $BN_{0.25}G_{0.75}$ shows electron transfer of 3.8 per oxygen molecule. The kinetic current density (i_k) values at –0.4 V versus SCE of $BN_{0.25}G_{0.75}$ is –4.6 mA cm^{-2} which is higher than $BN_{0.5}G_{0.5}$, $BN_{0.75}G_{0.25}$, and carboxylated graphene which showed –2.9, –2.4, and –1.3 mA cm^{-2}, respectively. The present study demonstrates that addition of a small amount of BN to the graphene matrix enhances the ORR activity significantly.

3. Conclusions

In conclusion, we have successfully prepared composites of BN and graphene with different compositions by covalent cross-linking with amide bonds by using EDC coupling. The composites exhibit tunable resistivity depending on the composition. The composites, especially $BN_{0.25}G_{0.75}$, show microporisity and satisfactory performance with high stability as supercapacitor electrode material. The composite with higher graphene content is also a good catalyst for ORR. Clearly, covalent cross-linking can be employed as a strategy to generate novel composites with useful properties.

4. Experimental Section

Reagents and Precursors: All the chemicals used in synthesis were of high purity and obtained from commercial sources. DMF was pre-dried before reaction. Amine functionalized few-layer BN (≈1–4 layers) was prepared by mixing boric acid and urea in 1:48 molar ratio and heating in high purity ammonia atmosphere at 900 °C for 5 h.[10a] Graphite oxide (GO) was synthesized using modified Hummers method.[7a] GO was placed in an alumina boat inside a quartz tube and inserted in the heating zone of furnace at 1050 °C under constant N_2 flow to obtain the exfoliated graphene (EG). Carboxylate functionalized graphene was obtained by microwave irradiation. In a typical batch, 200 mg EG was placed in 125 mL microwave reactor, 8 mL conc. HNO_3, 8 mL conc. H_2SO_4, 64 mL deionized H_2O was added and irradiated with microwave for 10 min at 450 W followed by heating in an oven at 100 °C for 12 h.[9] Obtained product was filtered using 0.45 µm polytetrafluroethylene (PTFE) membrane, washed with copious amount of water to remove excess acid and dried at 100 °C.

Synthesis of $BN_{1-x}G_x$ Composites Using EDC Coupling: Three different composites $BN_{1-x}G_x$ ($x \approx 0.25$, 0.5, and 0.75) were obtained by varying the ratio of BN with respect to carboxylated graphene. In a Schlenck flask, 150 mg of BN and carboxylated graphene was mixed in appropriate ratio, purged with N_2, sealed using septum and 35 mL DMF was added. Uniform dispersion was obtained by sonication. In the uniform dispersion *N*-(3-dimethylaminopropyl)-*N*′-ethyl-carbodiimidehydrochloride (EDC.HCl) 80 mg, 1-hydroxybenzotriazole (HOBt) 80 mg, and *N,N*-diisopropylethylamine (DIPEA) 1.2 mL was added under constant stirring and allowed for 48 h. Nitrogen atmosphere was maintained during the reaction. Obtained product was

filtered using 0.45 μm PTFE membrane, washed with copious amount of DMF and water. The solid product was further washed with methanol in a Soxhlet extractor for 48 h and dried at 100 °C under vacuum. Further, $BN_{1-x}G_x$ samples were annealed at 300 °C in N_2 atmosphere for 6 h and IR spectra was recorded to monitor the loss of amide bond between BN and graphene.

Electrochemical Measurements–Supercapacitor: Supercapacitor measurements were performed on PGSTAT 262 A (Techno Science Instruments) electrochemical workstation in 2 M H_2SO_4 aqueous electrolyte. Three-electrode assembly was used with a catalyst coated glassy carbon electrode (GCE) as the working electrode (WE), large-area Pt foil, and SCE as counter and reference electrodes, respectively. The working electrode was fabricated by dispersing 3 mg of sample in 1 mL ethanol–water mixture (1:1) and dropcasting 10 μL on GCE followed by 10 μL of 0.05 wt% nafion solution as binder. The electrodes were dried at 60 °C. CV measurements were carried out at different scan rates from 2 to 100 mV s^{-1}. EIS measurements were studied by applying an AC voltage with 10 mV amplitude in the frequency range from 0.1 Hz to 100 kHz. A GCD test was also conducted at different current densities. The specific capacitance (C_{sp}) was calculated using the following formula from CV, $C_{sp} = (i_+ - i_-)/(m \times \text{scan rate})$. Where, i_+ and i_- are the maximum values of current in the positive scan and negative scan respectively and m is the mass of single electrode. Specific capacitance was calculated from galvanostatic charge–discharge curves using the formula, $C_{sp} = (i)(dt)/(m \times dv)$.

Oxygen Reduction Reaction: A standard three-electrode cell with Pt plate as the counter electrode was used for the ORR study. For the oxygen reduction reaction, the catalyst was prepared by dispersing the catalyst (5 mg) in 1 mL mixture of ethanol and water in the presence of 0.05 wt% nafion. From this solution, 4 μL catalyst ink was drop casted on a GCE (3 mm diameter). Electrochemical measurements were performed in an O_2-saturated aqueous 0.1 M potassium hydroxide (KOH) solution (SCE reference electrode). Rotating disc electrode (RDE) measurements were carried out with a system from Beckman instruments, USA by coupling with a galvanostat/potentiostat PGSTAT 262A, Techno Science Instruments, Bangalore. The number of electrons transferred per oxygen molecule from the $BN_{1-x}G_x$ modified electrode can be calculated by using the Koutechy–Levich equation:

$$1/I = 1/i_k + 1/i_d \quad (1)$$

$$1/i = -1/(nFkC_o) - 1/(0.62nFD_o^{2/3}\gamma^{-1/6}C_o\omega^{1/2}) \quad (2)$$

Here, I denote the measured current densities at the respective potentials, whereas i_k and i_d represent kinetic and diffusion current densities respectively and n gives the overall number of electrons transferred per O_2 molecule. F is the Faraday constant (96 485 C mol^{-1}), C_o the bulk concentration of O_2 (1.2×10^{-6} mol mL^{-1}), k the electron transfer rate constant, D_o the O_2 diffusion coefficient (1.73×10^{-5} cm^2 s^{-1}) in 0.1 M KOH, γ kinematic viscosity (0.0109 cm^2 s^{-1}), and ω the rotation speed of the electrode. The number of electrons transferred, n, is obtained by calculating the slope of i^{-1} versus ω^{-1} plot.

The kinetic current density was calculated by the equation

$$i_k = (i \times i_d)/(i_{d-i}) \quad (3)$$

where i_k is the kinetic current density, i_d is the measured diffusion limited current density, and i is the measured current density.

Instrumentation and Characterization: Fourier transform infrared spectra (FTIR) were recorded in a Bruker FTIR spectrometer using attenuated-total-reflectance accessories. Raman spectra were recorded at several different spots in backscattering geometry using 514.5 nm Ar^+ laser in HORIBA LabRam HR800 spectrometer. Solid state ^{13}C MAS NMR spectrum was collected in Bruker AVANCE 400 MHz spectrometer. Elemental mapping using energy-dispersive X-ray spectroscopy and scanning electron microscope images were obtained using Nova Nano SEM 600, FEI. TEM images were collected using the FEI Tecnai with an accelerating voltage of 200 kV. Electron energy loss spectra were recorded in Titan FEI, TEM with an accelerating voltage of 300 kV. TGA was performed using Mettler Toledo TGA 850 in oxygen atmosphere with a heating rate of 3 °C min^{-1}. XPS were collected in an Omicron Nanotechnology Spectrometer with Mg Kα as the X-ray source. PXRD pattern was recorded in Bruker diffractometer using Cu K-α radiation. The N_2 sorption isotherm at 77 K was obtained using QUANTACHROME QUADRASORB-*SI* analyzer. The samples were heated at 383 K under vacuum for 12 h prior to the measurement of isotherm. Electrical resistivity was obtained using four-probe method on the composite pellets in physical property measuring system by Quantum design. Four equidistant linear contact points of gold was made over 8 mm composite pellet using radio frequency (RF) sputtering. Copper wires were connected to these gold contact points using silver paste.

Supporting Information

Supporting Information is available from the Wiley Online Library or from the author.

Received: May 27, 2015
Revised: July 27, 2015
Published online: September 10, 2015

[1] a) A. Pakdel, Y. Bando, D. Golberg, *Chem. Soc. Rev.* **2014**, *43*, 934; b) C. N. R. Rao, A. K. Sood, K. S. Subrahmanyam, A. Govindaraj, *Angew. Chem. Int. Ed.* **2009**, *48*, 7752.
[2] a) L. Song, Z. Liu, A. L. M. Reddy, N. T. Narayanan, J. Taha-Tijerina, J. Peng, G. Gao, J. Lou, R. Vajtai, P. M. Ajayan, *Adv. Mater.* **2012**, *24*, 4878; b) N. Kumar, K. Moses, K. Pramoda, S. N. Shirodkar, A. K. Mishra, U. V. Waghmare, A. Sundaresan, C. N. R. Rao, *J. Mater. Chem. A* **2013**, *1*, 5806.
[3] a) K. Raidongia, A. Nag, K. P. S. S. Hembram, U. V. Waghmare, R. Datta, C. N. R. Rao, *Chem. Eur. J.* **2010**, *16*, 149; b) L. Ci, L. Song, C. Jin, D. Jariwala, D. Wu, Y. Li, A. Srivastava, Z. F. Wang, K. Storr, L. Balicas, F. Liu, P. M. Ajayan, *Nat. Mater.* **2010**, *9*, 430; c) A. Pakdel, X. Wang, C. Zhi, Y. Bando, K. Watanabe, T. Sekiguchi, T. Nakayama, D. Golberg, *J. Mater. Chem.* **2012**, *22*, 4818.
[4] K. Moses, S. N. Shirodkar, U. V. Waghmare, C. N. R. Rao, *Mater. Res.* **2014**, *1*, 025603.
[5] a) M. P. Levendorf, C.-J. Kim, L. Brown, P. Y. Huang, R. W. Havener, D. A. Muller, J. Park, *Nature* **2012**, *488*, 627; b) K. Zhang, F. L. Yap, K. Li, C. T. Ng, L. J. Li, K. P. Loh, *Adv. Funct. Mater.* **2014**, *24*, 731.
[6] G. Gao, W. Gao, E. Cannuccia, J. Taha-Tijerina, L. Balicas, A. Mathkar, T. N. Narayanan, Z. Liu, B. K. Gupta, J. Peng, Y. Yin, A. Rubio, P. M. Ajayan, *Nano Lett.* **2012**, *12*, 3518.
[7] a) R. Kumar, V. M. Suresh, T. K. Maji, C. N. R. Rao, *Chem. Commun.* **2014**, *50*, 2015; b) R. Kumar, C. N. R. Rao, *J. Mater. Chem. A* **2015**, *3*, 6747.
[8] a) K. Gopalakrishnan, A. Govindaraj, C. N. R. Rao, *J. Mater. Chem. A* **2013**, *1*, 7563; b) K. Gopalakrishnan, K. Moses, A. Govindaraj, C. N. R. Rao, *Solid State Commun.* **2013**, *175*, 43.
[9] K. S. Subrahmanyam, S. R. C. Vivekchand, A. Govindaraj, C. N. R. Rao, *J. Mater. Chem.* **2008**, *18*, 1517.
[10] a) A. Nag, K. Raidongia, K. P. S. S. Hembram, R. Datta, U. V. Waghmare, C. N. R. Rao, *ACS Nano* **2010**, *4*, 1539; b) C. Zhi, Y. Bando, C. Tang, S. Honda, K. Sato, H. Kuwahara, D. Golberg, *Angew. Chem. Int. Ed.* **2005**, *44*, 7932; c) T. Sainsbury, T. Ikuno, D. Okawa, D. Pacilé, J. M. J. Fréchet, A. Zettl, *J. Phys. Chem. C* **2007**, *111*, 12992.
[11] a) E. Valeur, M. Bradley, *Chem. Soc. Rev.* **2009**, *38*, 606; b) C. A. G. N. Montalbetti, V. Falque, *Tetrahedron* **2005**, *61*, 10827.
[12] a) H. K. Schmid, *Micros. Microanal. Microstruct.* **1995**, *6*, 99; b) R. Arenal, M. Kociak, N. J. Zaluzec, *Appl. Phys. Lett.* **2007**, *90*, 204105.

[13] a) B. M. Kincaid, A. E. Meixner, P. M. Platzman, *Phys. Rev. Lett.* **1978**, *40*, 1296; b) R. D. Leapman, P. L. Fejes, J. Silcox, *Phys. Rev. B* **1983**, *28*, 2361.
[14] K. A. Mkhoyan, A. W. Contryman, J. Silcox, D. A. Stewart, G. Eda, C. Mattevi, S. Miller, M. Chhowalla, *Nano Lett.* **2009**, *9*, 1058.
[15] a) X. Gouin, P. Grange, L. Bois, P. L'Haridon, Y. Laurent, *J. Alloys Compd.* **1995**, *224*, 22; b) H. A. Castillo, P. J. Arango, J. M. Vélez, E. Restrepo-Parra, G. Soto, W. D. la Cruz, *Surf. Coat. Technol.* **2010**, *204*, 4051.
[16] a) Z.-J. Fan, W. Kai, J. Yan, T. Wei, L.-J. Zhi, J. Feng, Y.-M. Ren, L.-P. Song, F. Wei, *ACS Nano* **2011**, *5*, 191; b) T. Ramanathan, F. T. Fisher, R. S. Ruoff, L. C. Brinson, *Chem. Mater.* **2005**, *17*, 1290.
[17] P. S. Marchetti, D. Kwon, W. R. Schmidt, L. V. Interrante, G. E. Maciel, *Chem. Mater.* **1991**, *3*, 482.
[18] a) V. Nicolosi, M. Chhowalla, M. G. Kanatzidis, M. S. Strano, J. N. Coleman, *Science* **2013**, *340*; 1226419; b) C. Zhi, Y. Bando, C. Tang, H. Kuwahara, D. Golberg, *Adv. Mater.* **2009**, *21*, 2889.
[19] Y. Gu, M. Zheng, Y. Liu, Z. Xu, *J. Am. Ceram. Soc.* **2007**, *90*, 1589.
[20] D. W. Mayo, F. A. Miller, R. W. Hannah, in *Course Notes on the Interpretation of Infrared and Raman Spectra*, John Wiley & Sons, Inc, Hoboken, NJ **2004**.
[21] a) S. Saha, D. V. S. Muthu, D. Golberg, C. Tang, C. Zhi, Y. Bando, A. K. Sood, *Chem. Phys. Lett.* **2006**, *421*, 86; b) J. Wu, W.-Q. Han, W. Walukiewicz, J. W. Ager, W. Shan, E. E. Haller, A. Zettl, *Nano Lett.* **2004**, *4*, 647.
[22] L. M. Malard, M. A. Pimenta, G. Dresselhaus, M. S. Dresselhaus, *Phys. Rep.* **2009**, *473*, 51.
[23] K. S. W. Sing, D. H. Everett, R. A. W. Haul, L. Moscou, R. A. Pierotti, J. Rouquerol, T. Siemieniewska, *Pure Appl. Chem.* **1984**, *57*, 603.